Laplace inverted pulsed EPR relaxation to study contact between active material and carbon black in Li-organic battery cathodes

Davis Thomas Daniel[1,2,*],Conrad Szczuka[1], Peter Jakes[1], Rüdiger-A. Eichel[1,3], Josef Granwehr [1,2]

[1]Institute of Energy and Climate Research (IEK-9), Forschungszentrum Jülich, Jülich 52425, Germany

[2] Institute of Technical and Macromolecular Chemistry, RWTH Aachen University,Aachen 52056, Germany

[3] Institute of Physical Chemistry, RWTH Aachen University,Aachen 52056, Germany

**Correspondence to: d.daniel@fz-juelich.de*

Abstract

The addition of conductive additives during electrode fabrication is standard practice to mitigate a low intrinsic electronic conductivity of most cathode materials used in Li-ion batteries. To ensure an optimal conduction pathway, these conductive additives, which generally consist of carbon particles, need to be in good contact with the active compounds. Herein, we demonstrate how a combination of pulsed electron paramagnetic resonance (EPR) relaxometry and inverse Laplace transform (ILT) can be used to study such contact. The investigated system consists of PTMA (poly(2,2,6,6–tetramethylpiperidinyloxy–4–ylmethacrylate)) monomer radicals, which is a commonly used redox unit in organic radical batteries (ORB), mixed at different ratios with Super P carbon black (CB) as the conductive additive. Inversion recovery data were acquired to determine longitudinal, or T_1, relaxation time constant distributions. It was observed that not only the position and relative amplitude, but also the number of relaxation modes varies as the composition of PTMA monomer and CB is changed, thereby justifying the use of ILT instead of fitting with a predetermined number of components. A hypothesis for the origin of different relaxation modes was devised. It suggests that the electrode composition may locally affect the quality of electronic contact between the active material and carbon black.

Introduction

Improving the energy density of Li-ion batteries is of vital importance for meeting next-generation energy storage needs.[1,2] A commonly proposed solution is to reduce the amount of inactive components such as conductive additives or binders in the battery.[3] Conductive additives are necessary to improve the bulk electronic conductivity of electrodes, since most of the electrode materials utilized in Li-ion batteries exhibit low intrinsic electronic conductivity.[4] However, since the conductive additives do not contribute to the capacity of the battery in most cases, the amount of additive in the electrode needs to be optimized. This aspect is particularly crucial for advancing sustainable battery technologies, such as organic radical polymer batteries (ORB),[5] where conductive additives are used in significant amounts.[6,7] ORB cathodes with up to 70 wt-% of conductive additive have been reported.[8] For instance, PTMA (poly(2,2,6,6-tetramethylpiperidinyloxy-4-ylmethacrylate)), a commonly employed radical polymer, exhibits limited electrical conductivity and requires up to 50 wt-% of conductive additive for optimal performance.[9,10]

Electrochemical performance of ORBs utilizing PTMA as the active material is significantly affected by the type and amount of conductive additive used,[11–13] highlighting the need for optimization of electrode composition. The electron transfer mechanism in PTMA based ORBs involves a two step process – electron transfers between the redox active units on the polymer backbone, and electron transfer through the conductive additive.[14] A continuous conduction pathway between active material, conductive additive, and current collector is necessary for electrochemical accessibility and high electronic conductivity. In particular, interfacial contacting between redox active units and carbon additives may be a conductivity bottleneck[11,15] that has been shown to influence the overall battery performance.[16,17] For ORB active materials that feature an insulating polymer backbone, such as PTMA, a disruption in the contact at the interface between current collector and conductive additive can be caused by the polymer backbone itself, leading to low intrinsic conductivity.[14,18] Investigating the electronic contact between the active material and the conductive additive could reveal conductivity bottlenecks and aid in optimizing the electrode composition. Therefore, a generally applicable technique to study such contact in composite electrode materials is desirable.

Electron paramagnetic resonance (EPR) is a spectroscopic technique to investigate the environment and dynamics of unpaired electrons in materials. Since the redox states in batteries often involve unpaired electrons, EPR can be utilised to investigate these systems. With respect to battery materials, continuous wave EPR (CW EPR) is often used to confirm the presence of unpaired electrons and for quantification of radical density.[6,19,20] Moreover, pulsed EPR techniques,[21–24] *in operando* CW EPR[25] and EPR imaging[26,27] for battery research have also been demonstrated. PTMA based ORBs consist of nitroxide radicals as the redox active unit, which are well-characterized using EPR[28] at low concentrations. EPR spectroscopic investigations of PTMA mainly utilize CW EPR techniques, as densely packed nitroxide radicals make the application of

advanced EPR techniques challenging. Due to spin exchange interaction between the radicals,[29] the EPR line broadens initially and starts narrowing after exceeding the slow exchange limit, leading to a loss in resolution of ^{14}N hyperfine features. High spin concentration and spatially close nitroxide radicals on the polymer chain also lead to shortening of the relaxation times, making the system less amenable to pulsed EPR techniques.

For ORBs with nitroxide radicals as redox units, *in situ*[30] and *in operando*[22] CW EPR have shown the presence of electrochemically inactive radicals on the cathode film. The presence of such inactive redox centres, which do not undergo a change in their redox states while charging or discharging, inhibits the maximum attainable capacity of the ORB. The formation of inactive redox centres in the cathode film could be a result of disruption in contact between the conductive additive and the active material during battery cycling,[31] disabling the isolated radicals from participating in the electrochemical reaction. In this case, insight into the distribution of these inactive radical centres and their interaction with the conductive additive could help in identifying important capacity-loss pathways.

The distribution of paramagnetic centres (aggregated or sparsely distributed) and their interaction with the environment can be accessed through their spin relaxation behaviour.[32,33]Measurement of the spin–lattice relaxation time constant, T_1, is mainly done using inversion or saturation recovery techniques. In saturation recovery, the populations of all EPR levels are equalized with a long microwave excitation, followed by a detection sequence that measures the recovery of equilibrium magnetization. Inversion recovery uses a π pulse to invert the longitudinal magnetization, and after a variable delay a spin echo sequence is used to monitor its recovery towards equilibrium.

In addition to true T_1 relaxation, which involves an exchange of energy between the spin system and its environment (lattice), apparent relaxation may also contribute to relaxation measurements. In an inversion recovery experiment of samples with a broad EPR spectrum, the bandwidth of the microwave pulse may only suffice to excite a small fraction of spins. Processes such as molecular motions, electron spin exchange and spin flip-flops of nearby spins can transfer magnetization to spins which are not directly excited, leading to apparent relaxation through spectral diffusion. Spectral diffusion is known to contribute primarily to inversion recovery, but saturation recovery is only unaffected when using saturation sequences with a duration on the order of T_1.[34] In this work, inversion recovery, which offers a higher sensitivity than saturation recovery, is used to obtain T_1 relaxation curves.

Different paramagnetic species exhibit varied relaxation behaviour.[35] While nitroxide radicals represent a spin system with localized unpaired electrons, conductive additives such as carbon blacks may have contributions from both localized paramagnetic defect centres and mobile conduction electrons,[36,37] allowing the use of EPR techniques for their characterization.[36–41] Conduction electrons and nitroxide radicals can be distinguished according to their line shape,[42,43] but also differ in their relaxation characteristics. In case of conduction electrons, $T_1 \approx T_2$ is often found.[41,43,44] For immobilized nitroxide

radicals, $T_1 \gg T_2$ is commonly observed.[45,46] In mixed electronic systems, such as the ones investigated in this work, exchange interactions between localized and delocalized electrons serve as an efficient relaxation pathway for the localized electrons.[47–50] Nitroxide radicals that interact with faster relaxing electron spins in their vicinity have been reported to undergo similar relaxation enhancement through exchange or dipolar interactions,[51,52] enabling the determination of parameters such as inter-spin distances.[53] The interaction strength of a nitroxide radical with a carbon black conduction electron, therefore, can be inferred from the relaxation enhancement of the nitroxide radical.

The microscopically heterogeneous nature of nitroxide based active material and carbon black composite samples, with potentially varying grades of contact quality, may cause a distribution of relaxation time constants rather than a single relaxation time. In order to obtain relaxation time distributions, inversion algorithms are suitable, especially in cases where the number of relaxation components is unknown. In order to stabilize the solution of such an inversion, regularization techniques such as Tikhonov regularization can be employed. While Tikhonov regularization is widely used in EPR for the calculation of distance distributions,[54] it has not found widespread application for the analysis of relaxation data. Since most time-domain EPR relaxation studies are conducted on solid samples, negative contributions in the distribution cannot be excluded *a priori*.[55,56] Therefore, the commonly used non-negativity constraint to stabilize the ill-posed inversion with exponential kernel[57,58] may lead to inaccurate or unstable results. Employing a conventional fitting technique using, for example, a mono-exponential, stretched exponential, or multi-exponential model, proves more robust and simpler to implement.[59] However, a combination of a uniform penalty regularization, which is less prone to wildly oscillating solutions of inversions with exponential kernel than Tikhonov regularization in standard form,[60] and a zero-crossing penalty proved to be a suitable alternative.[61] Thereby, uncertainty of the results is represented as linewidth.[62] The aim of the inversion is to find the broadest possible relaxation modes that fit the experimental data without showing non-random, systematic residuals.[63]

Herein, we demonstrate the use of pulsed EPR relaxometry in combination with Laplace inversion, or inverse Laplace transform (ILT), to study the quality of electronic contact in a composite electrode system. The composite system consists of PTMA monomer, shown in Figure 1, as the active material, and Super P carbon black (CB) as the conductive additive. Super P mainly consists of spherical carbon particles that form a conductive network within the composite electrode.[64,65] The PTMA monomer to CB weight ratio (PMCR) was varied systematically in the composite samples. Continuous-wave (CW) EPR was used to identify the number and distribution of paramagnetic centres, and pulsed EPR was employed to probe the relaxation characteristics of the active material. Laplace inversion of the relaxation data was used to afford relaxation distributions and establish correlations between the composition and the quality of PTMA monomer-CB contact.

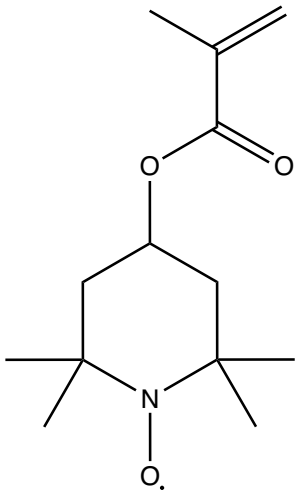

Figure 1: Chemical structure of PTMA monomer

Experimental

Sample preparation

Composite samples of PTMA (poly(2,2,6,6-tetramethylpiperidinyloxy-4-ylmethacrylate)) monomer (Sigma Aldrich, Germany) and Super P carbon black (Alfa Aesar, Germany) were prepared by adding nitroxide solutions in toluene to the Super P powder. The amount of solution added to CB was kept constant at 100 µL for all samples. The nitroxide concentration was adjusted to obtain the desired weight ratios. The samples were then dried at 60 °C for two weeks in an oven under air, followed by crushing the samples using a mortar and pestle to obtain a fine powder. The powder samples were transferred to 2 mm outer diameter EPR tubes and filled to a height of 30 mm. The 'wet' composite samples were obtained by adding 50 µL of toluene to dried composite samples within the EPR tube. The EPR tube was left undisturbed until the solvent fully permeated and soaked the sample.

EPR spectroscopy

CW EPR : X-Band CW EPR spectra were recorded using a Bruker Elexsys E540 EPR spectrometer operating at 9.33 GHz. The spectra were recorded at room temperature as first derivatives of the absorption function, with a field modulation amplitude of 0.05 mT, modulation frequency of 100 kHz, and microwave power of 0.6325 mW.

Pulsed EPR : All pulsed EPR experiments were conducted on a Bruker ELEXSYS E580 X-band spectrometer with a Bruker EN 4118-X-MD4 pulse ENDOR resonator. The tem-

perature was maintained at cryogenic levels with a helium cryostat (Oxford Instruments, CF935). For experiments at cryogenic temperatures, the samples were flash frozen using liquid nitrogen and then inserted into the cryostat. The $\pi/2$ and π pulse lengths were set to 16 ns and 32 ns respectively. Field swept echo detected EPR spectra were acquired using a standard two-pulse Hahn echo sequence with an inter-pulse delay τ of 200 ns. For T_1 measurements, an inversion recovery sequence (π – t_R – $\pi/2$ – τ – π – τ – echo) with a 4-step phase cycle[66] was used. τ was kept at 200 ns and the initial delay t_R after inversion was set to 400 ns, which was incremented linearly in steps of 1.5 µs to obtain an inversion recovery time trace with 512 points.

Laplace Inversion

T_1 relaxation time distributions were obtained using Laplace inversion with an exponential kernel, where the measured signal s_k of the k^th recovery data point was represented as

$$s_k = \sum_{l=0}^{M} \exp\left(-\frac{t_{\mathrm{R},k}}{T_{1,l}}\right) g_l \,. \tag{1}$$

$T_{1,l}$ with $l > 0$ is the l^th element of a user-selected, logarithmically spaced relaxation time vector of size M, and $T_{1,0}^{-1} = 0$ represents the equilibrium baseline signal obtained for infinite recovery delays, $t_\mathrm{R} \to \infty$. g_l are the elements of the fitted relaxation time distribution vector $\mathbf{g}$. For the inversion of Equation 1, a uniform penalty regularization and an additional penalty for zero-crossing of the density function is used instead of a non-negativity constraint to stabilize the result. Parametrization was done without adjustable parameters by matching the norm of the regularization parameter with an estimate of the norm of the random noise of the data. Details of the algorithm and parametrization are as described elsewhere.[61] Prior to inversion, the noise level was estimated by subtracting a linear fit of data points near the end of the t_R time trace. The raw data was then scaled to unity variance using the estimated noise level. Inversion recovery curves may exhibit non-zero baselines, which may be interpreted by the algorithm as a slow relaxing component. This artefact manifests in the obtained relaxation distribution as peak with a long relaxation time constant. In the relaxation distributions shown in this work, this baseline artefact is avoided by adding an additional data point to the time trace and fitting the baseline as a single value. Laplace inversion was performed using home-written scripts that were run on Octave 6.4.[67]

Results and discussion

CW EPR

Figure 2a shows the CW EPR spectra for a series of PTMA monomer–CB composite samples. The ratios on the right edge of each spectrum denote the PTMA monomer to CB weight ratio (PMCR). Hereafter, the composite samples are referred by their respective PMCR. The topmost spectrum is the one of neat CB (marked as Super P). The CB spectrum is characterized by a symmetrical Lorentzian line with $g = 2.0023$ and a peak-to-peak linewidth of $\Delta B = 0.54$ mT. The line narrows to 0.35 mT upon treatment with solvent or evacuation. Exchange interaction of CB electrons and paramagnetic molecular oxygen causes the EPR line of CB to broaden, and treatment with solvent displaces the paramagnetic oxygen from CB surfaces resulting in a narrower line. Similar behaviour of the EPR line has been reported for various carbon blacks.[36,40,68]

In comparison to neat CB, the spectra of composite samples showed a narrower linewidth of $\Delta B = 0.35$ mT for the CB component, indicating that the CB conduction electrons do not undergo exchange with paramagnetic oxygen in these samples. This suggests that CB interfaces in the composite samples are not exposed to molecular oxygen, possibly due to residual solvent or being coated by the PTMA monomer. For the nitroxide component, a broad EPR line was observed in 2:1, owing to spin exchange interactions between nitroxide radicals. This is indicative of densely packed nitroxide radicals. The intensity of this broad nitroxide component decreases as the relative amount of PTMA monomer decreases, and it is resolved to a lesser extent in 1:1. For composite samples with a higher relative amount of CB than 1:1, the nitroxide component was not resolved. For PMCR of 1:6, 1:20 and 1:30, the spectral features were similar to a PMCR of 1:2, and only the contribution from CB was resolved.

The broadening of the nitroxide EPR line in 1:1 and the absence of a resolved nitroxide component for samples with a higher relative amount of CB could be a result of relaxation rate enhancement of nitroxides in the presence of CB. Linewidth in CW EPR spectra is dependent on relaxation, where a short spin–spin relaxation time T_2 leads to EPR line broadening. Stochastic collisions between paramagnetic centres is known to cause relaxation enhancement through spin exchange interaction.[34,46] In the composite samples, relaxation enhancement of the nitroxide radicals could be afforded through frequent encounters with mobile conduction electrons of CB, shortening the longitudinal relaxation time T_1 due to exchange interactions.[49,53] In 2:1, the densely packed nitroxides seem to be sufficiently isolated from the CB, such that the relaxation is slower and the nitroxide component is resolved. In contrast, in 1:1 and the samples with higher relative amount of CB, a better dispersion of nitroxide radicals improves the accessibility of the radicals towards CB and increases the probability of encounter with conduction electrons. This results in a severe broadening of the nitroxide EPR line.

In order to confirm that the absence of the nitroxide component was not a result of a chemical change of the radical centre due to the heat treatment (see Sample preparation)

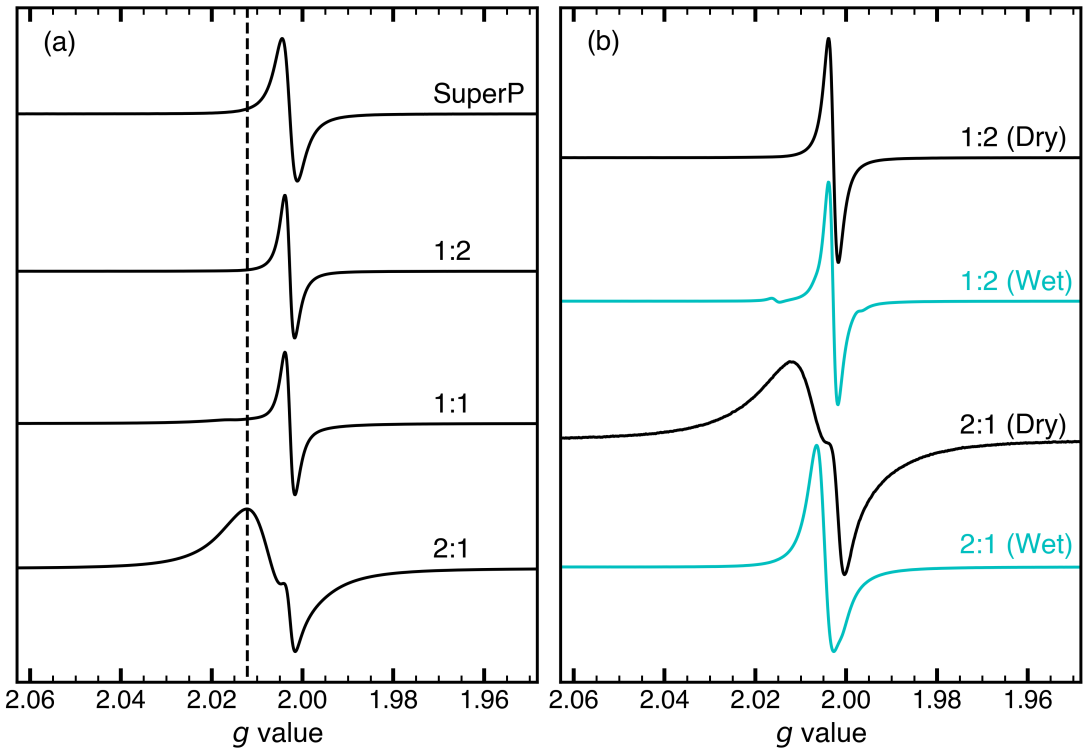

Figure 2: X-band (9.33 GHz) continuous wave EPR spectra of composite samples acquired at 295 K with a modulation amplitude of 0.05 mT and modulation frequency of 100 kHz. Ratios on the right edge of each spectrum denotes the PMCR. (a) EPR spectra of composite samples with varying PMCR compared to neat CB (Super P). The dashed line denotes the contribution from the nitroxide species. (b) Comparison of EPR spectra of wet (cyan) and dry (black) composite samples. The characteristic three line EPR spectrum of the nitroxide species is observed (feature at $g = 2.015$).

or addition of CB, solvent was re-introduced to the dry composite samples. Upon addition of solvent, 'wet' 2:1 (see Figure 2b) showed a narrower linewidth of the nitroxide EPR component, consistent with a reduced contact between the nitroxide radicals and the CB in the presence of a solvent. In 1:1 and in samples with a higher relative amount of CB (see wet 1:2 spectrum in Figure 2b), a characteristic three-line spectrum of nitroxide was observed. The results indicate that the nitroxide radical centre remains chemically intact in the composite sample, but the relaxation properties are considerably altered by the CB.

Pulsed EPR

Pulsed EPR was employed to characterize the relaxation behaviour of the PTMA monomer in the presence of CB. For all the composite samples investigated, a spin echo from the nitroxide component was obtained only below 60 K. No spin echo was obtained at the same experimental conditions for the neat CB sample. Field-swept echo detected EPR spectra for composite samples recorded at 50 K were typical of immobilized nitroxide radicals[69] (Figure 3b). For the same τ delay, the relative intensity of the central $m_I = 0$ transition compared to $m_I = 1$ and $m_I = -1$ transitions was found to decrease as the amount of nitroxide in the composite sample was increased. This effect is attributed to instantaneous diffusion,[34,70–72] which is proportional to spin concentration and is indicative of a network of dipole–dipole coupled spins.[34] Since dipole–dipole coupling is distance dependent, the spectral shape of echo detected spectra is indicative of the packing density of the nitroxide radicals in the composite sample.

The echo detected spectral shape for 2:1 is consistent with a dense packing of nitroxide radicals, while the nitroxides are spatially more distant in 1:2. For a PMCR of 1:6, 1:20 and 1:30, the spectral features were similar to that of 1:2. τ-filtered echo detected spectrum of 2:1 revealed an additional component at $g = 2.0017$ for a τ value of 484 ns. Considering the narrow width of the feature and its proximity to the free electron g value, this feature likely originates from a coalescence of spectral features due to exchange interactions.

A distinction between different nitroxide relaxation components as a result of spin exchange with CB was not apparent from the EPR spectrum directly (compare 1:2 and 1:20 in Figure 3b). The spectral shape of the nitroxide was preserved. Therefore, either the exchange interaction between the nitroxide radicals and CB was not strong enough to cause exchange narrowing, or radicals in close proximity to CB, which experience a strong exchange interaction, contributed negligibly to the spin echo. The latter is more likely, as in the strong exchange limit a nitroxide radical in the vicinity of a faster relaxing paramagnetic species will have a relaxation rate approaching that of the fast-relaxing species.[53]

Inversion recovery experiments for measuring T_1 were conducted at the field position of maximum intensity. Figure 4 shows the inversion recovery time traces for composite samples with varying PMCR. T_1 increases as the composition is changed from 2:1 to 1:2 and starts decreasing after 1:2. In 2:1, due to the dense packing of nitroxide radicals, the dominant contribution to relaxation is expected to be spin interactions between the nitroxide radicals, which account for the majority of the lattice. In addition, the relaxation curve might have contributions from spectral diffusion processes,[34] which are prominent in aggregated spin systems with small inter-spin distances such as in 2:1. Spectral diffusion tends to shorten spin-lattice relaxation times.[53,70,73] As the nitroxides get more dispersed through the carbon lattice in 1:2, the aforementioned contributions decrease and T_1 increases from 2:1 to 1:2. The increase in T_1 from 2:1 to 1:2 indicates that the majority of nitroxide radicals exhibit relaxation, which is influenced by nitroxide–nitroxide

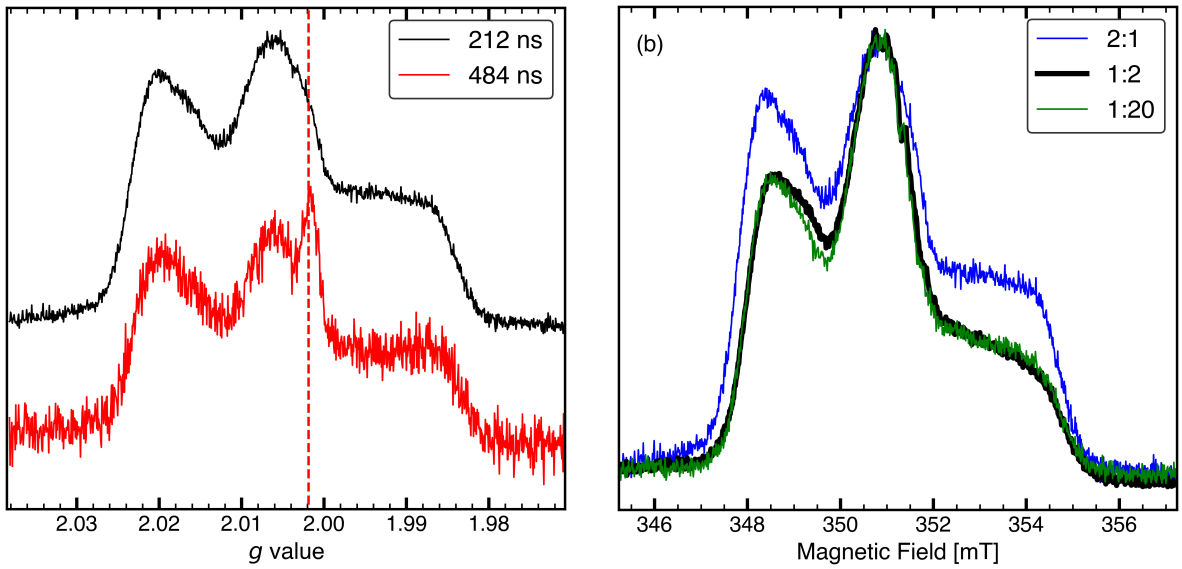

Figure 3: Field-swept echo-detected X-band EPR spectra of PTMA monomer-Super P composite samples at 50 K. The $\pi/2$ and π pulse lengths were set to 16 ns and 32 ns, respectively. (a) Echo-detected EPR spectra of a 2:1 sample with inter-pulse delay $\tau =$ 212 ns (black) and $\tau = 484$ ns (red). The black spectrum is vertically shifted for clarity. The echo-detected EPR spectrum with $\tau = 484$ ns shows a narrow feature near $g = 2.0017$ (red dotted line), likely originating from exchange interactions. (b) Echo-detected EPR spectra with $\tau = 200$ ns of samples with PTMA monomer-to-Super P ratio of 2:1 (blue), 1:2 (black), and 1:20 (green). Spectra are normalized to the amplitude of the central line. The spectral shape was similar for the 1:2 and 1:20 samples.

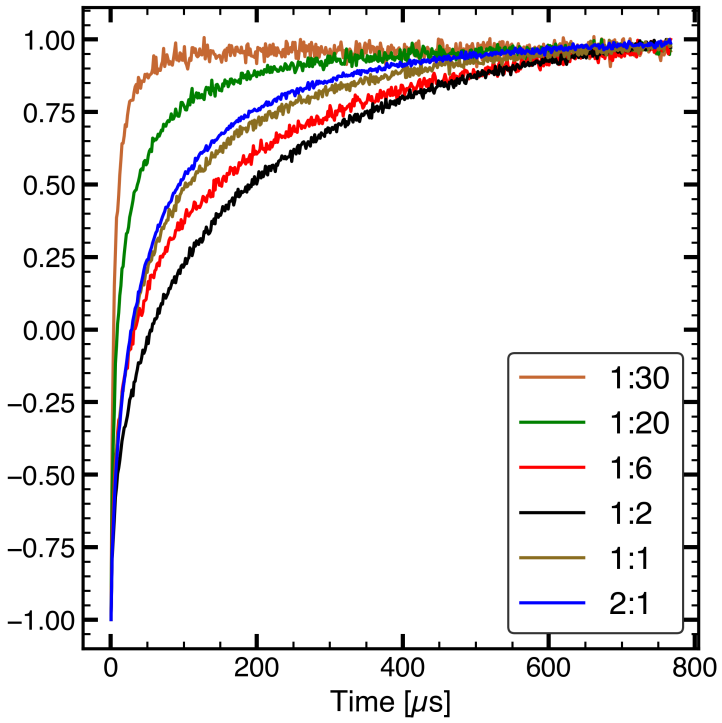

Figure 4: Comparison of inversion recovery time traces for varying ratios of PTMA monomer to Super P, acquired at 50 K. The 1:30 composite sample shows the fastest T_1 relaxation. While field-swept echo-detected EPR spectra of 1:2 and 1:20 were similar, T_1 relaxation shows a significant difference.

contact. Decreasing the number of nitroxide–nitroxide close contacts or increasing the distance slows the relaxation. In contrast, for 1:6, where CB accounts for most of the lattice, a further increase in dispersion of nitroxide radicals does not lead to a slower relaxation, suggesting that the nitroxide radicals are well-separated. The faster relaxation observed in 1:6 indicates a more efficient energy transfer between spin system and the lattice. From the perspective of CB, the conductive network is dependent on the inter-particle contact,[31,74] which improves as the PTMA monomer is more dispersed, allowing the formation of more continuous conduction pathways and a better dissipation of energy through the lattice. As the PTMA monomer–CB contact improves further in samples with PMCR below 1:6, T_1 decreases further.

The change in relaxation trend from 1:2 to 1:6 suggests that the dependence of relaxation on sample composition is not a simple monotonic correlation with the amount of CB. If the distribution of PTMA monomer within the CB lattice is non-uniform, the presence of distinct PTMA monomer populations differing in their contact quality with CB within the same composite sample is also possible. As evident when comparing relaxation curves of 2:1 and 1:30, relaxation of the nitroxide–nitroxide contact dominated system is significantly different from a system where nitroxide–CB contact is dominant. Therefore, a distribution in the quality of PTMA monomer–CB contact can be considered as a distribution in relaxation times.

Laplace Inversion

In order to obtain relaxation time distributions from time domain inversion recovery data, ILT was conducted. The possibility of multiple relaxation environments in the investigated system makes ILT an apt tool to be used here, as relaxation time distributions can be obtained without assuming the number of relaxation components. Figure 5 shows the T_1 relaxation time distributions obtained using ILT with an exponential kernel. The T_1 distributions did not show any physically implausible features or systematic artefacts, and the residuals from fits were representative of random noise devoid of any apparent systematic features (see Figure S1). The absence of non-random features in the residuals indicates that the chosen kernel is compatible with the data and Laplace inversion is able to accurately extract all the features from the T_1 experiment. Exchange features, such as contributions with a negative sign, were not apparent in the distributions, albeit exchange cannot be excluded either.

The distributions indicated at least two distinct relaxation components for each composite sample except for 1:30, where a fairly isotropic distribution was obtained. The two components differed by an order of magnitude in relaxation time values. The relaxation time values for the slow relaxing component ranged from 70 µs to 380 µs, while for the fast relaxing component, the values ranged from 1 µs to 10 µs. The relaxation trend observed from the inversion recovery curves were followed by both components, with an initial increase in T_1 from 2:1 to 1:2, followed by a decrease in the samples from 1:2 to 1:30. In

changing the composition from 2:1 to 1:30, the lattice changes from a nitroxide dominated environment in 2:1 to CB dominated environment in 1:30. This aspect is also reproduced in the relaxation distribution, where a uniform distribution is obtained for 1:30 with a distribution maximum that is close to the relaxation time of the fast relaxing species observed in 2:1. The similarity in the relaxation trend for both components suggests that the relaxation of each species is influenced by multiple relaxation processes. However, as evidenced by the large difference in relaxation time values, the relative weight of their contribution to relaxation for each component differs. In other words, within a sample the PTMA monomers in good contact with CB relax faster and are less sensitive to changes in the extent of nitroxide dispersion or nitroxide–nitroxide contact. In contrast, PTMA monomers that exist in densely packed clusters seem to relax more slowly and are more sensitive to changes in nitroxide dispersion.

In order to derive mean relaxation time constants and amplitudes, the distributions were fit using Gaussian functions in log space. Integrals from the Gaussian fits were utilized for a quantitative analysis of different relaxation components. Composite samples with PMCR of 2:1, 1:1, 1:20 and 1:30 could be satisfactorily fit with a two-Gaussian model, while a three-Gaussian model was required for 1:2 and 1:6.

For the 2:1 sample, the slow relaxation component is centred at 70 µs in the corresponding relaxation time distribution (see component **2** in Figure 5) while the fast relaxing component is centred at 1.7 µs, corresponding to PTMA monomers in good contact with CB. Upon decreasing the amount of nitroxide in 1:1, the contribution of nitroxide–nitroxide contact to relaxation decreases, indicated by the increase in T_1 values for both relaxation components (see component **1** and **2** in Figure 6b). The increase in T_1 is also accompanied by an increase in the amount of the fast relaxing component and a concomitant decrease in the slow relaxing component, indicating that the proportion of PTMA monomers in contact with CB has increased. As the PTMA monomers are dispersed further in 1:2 and 1:6, the fractions of nitroxides influenced by nitroxide–nitroxide contact and those influenced by nitroxide–CB contact become comparable. The corresponding distribution for 1:2 consist of three components, a fast relaxing component at 6 µs (**1** in Figure 5), an intermediate component at 111 µs (**2′** in Figure 5) and a slow relaxing component at 343 µs (**3** in Figure 5). Component 3 exhibits a larger T_1 value in 1:6, indicating that the PTMA monomers corresponding to component 3 are not influenced by the increase in the amount of CB, but are sensitive to the distribution of nitroxides or nitroxide–nitroxide contact. Component 1 and 2′ show a decrease in T_1 value in 1:6, consistent with a larger proportion of PTMA monomers in contact with CB. The change in relative amounts of **1**, **2′** and **3** in changing the composition from 1:2 to 1:6 is also consistent with an increased proportion of PTMA monomers interacting with CB. Although components **1** and **2′** are attributed to PTMA monomers interacting with CB, the strength of this interaction and therefore the quality of contact with CB for **1** and **2′** was found to be different. This is indicated by a considerable difference ($\approx$ 100 µs) in relaxation time values for **1** and **2′**.

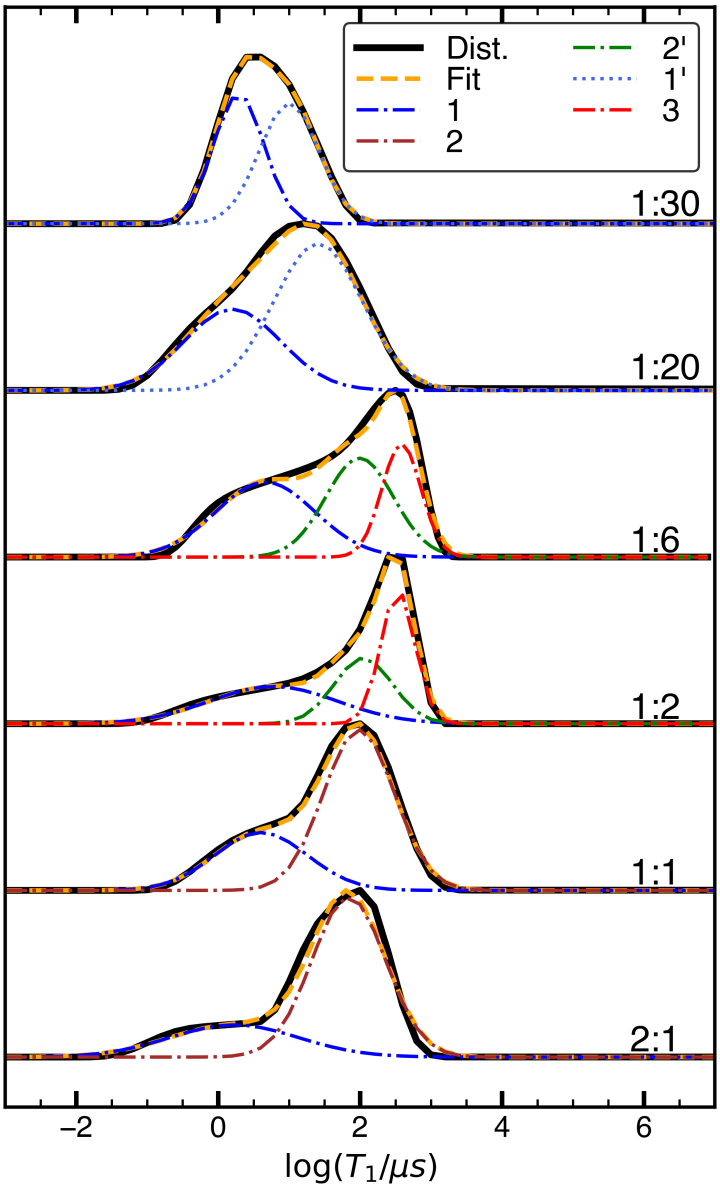

Figure 5: Relaxation time distributions (black) for varying PMCR. Inversion recovery experiments were conducted at 50 K. T_1 data were inverted using an exponential kernel to obtain the distributions. Labels on the right edge denote the PTMA monomer-to-Super P weight ratio. For quantitative analysis, the distributions were fit (orange) to Gaussian functions in log space. Refer to text for the discussion on individual components 1 (blue), 1′ (light blue), 2 (brown), 2′ (green) and 3 (red).

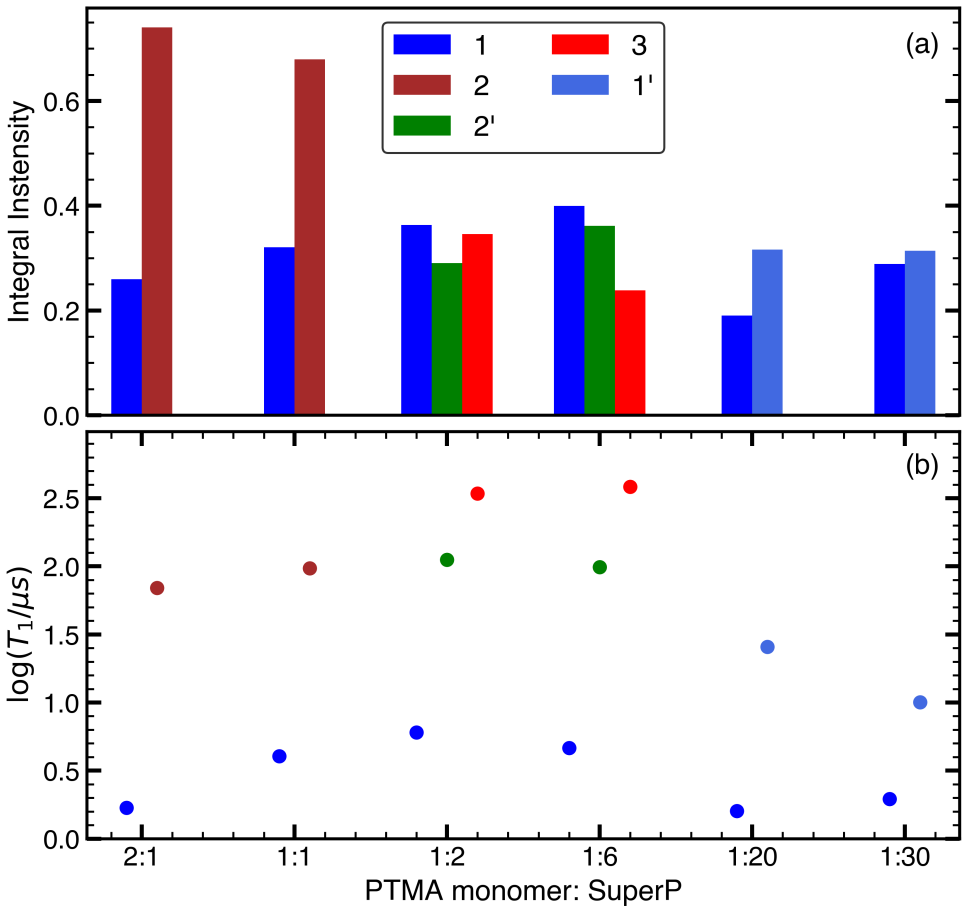

Figure 6: T_1 values and integrals obtained by fitting relaxation time distributions with Gaussian functions in log space. (a) Integrals of relaxations components shown in Figure 5. (b) T_1 values of relaxation components obtained from the mode of Gaussian fits shown in Figure 5.

Component **2′** likely represents a proportion of PTMA monomers that is influenced by both nitroxide–nitroxide contact and nitroxide–CB contact, the latter being more dominant. This could be the case if the PTMA monomers are present in smaller clusters and spread throughout the carbon lattice, leading to a weaker exchange interaction with CB in comparison to component **1**, which represents isolated radicals. In 1:20 and 1:30, a distinction between the slow and fast relaxing component is not as pronounced as in other compositions. For instance, in 1:30, the relaxation components only differ by 8 µs, (see components **1**, **1′** in Figure 6a), indicating a similar quality of contact with CB. Therefore, the increase in the relative amount of the fast relaxing component is maintained throughout the composition range on account of the PTMA monomers being increasingly dispersed and made accessible to the conductive network of CB.

A schematic model for the composite system based on the relaxation distributions is shown in Figure 7. Three different relaxation regimes corresponding to different degrees of PTMA monomer-CB contact are identified. The fastest relaxing component, **1**, is attributed to well dispersed PTMA monomers in good contact with CB. Component **2** is attributed to PTMA monomers which are likely present as smaller clusters leading to an intermediate contact quality with CB. The slowest relaxing component, **3**, is attributed to aggregated nitroxides in a poor contact with CB.

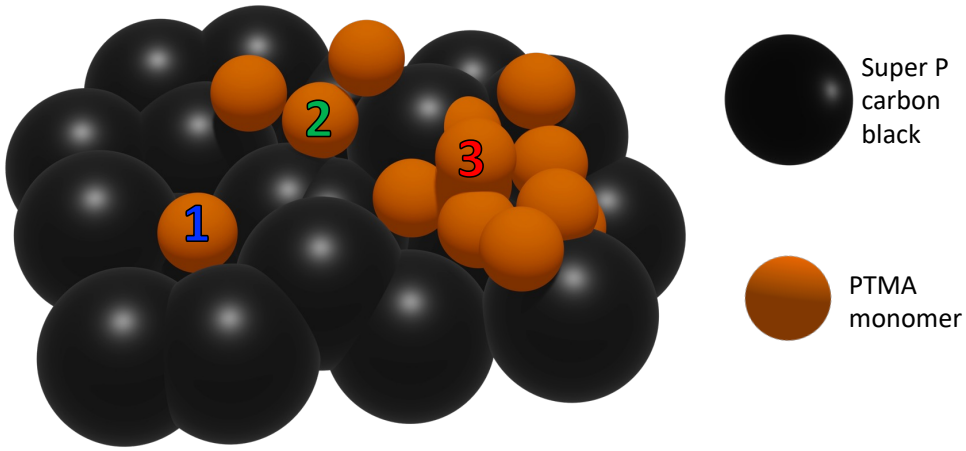

Figure 7: Proposed model for the PTMA monomer-Super P composite system based on the relaxation distributions obtained using ILT. Three different relaxation regimes are identified corresponding to the three relaxation components observed in the relaxation distributions.

The relaxation time constant distributions followed the same trends at 30 K, and a better resolution of the relaxation components was observed than at 50 K (see Figure S2). An improved resolution in the relaxation time distribution at lower temperature is likely due to different temperature dependencies of the relaxation components. Figure 8 shows a comparison of relaxation time distributions for 1:2 and 1:20 at 30 K, where an increase of the fast relaxing components (**1** and **2**) and a decrease in the slow relaxing component (**3**) is observed when decreasing the amount of nitroxides. For the same PMCR, the reproducibility of the relaxation components from separate data sets acquired at different temperatures was good and highlights the robustness of ILT as a method to study contact in battery materials.

Since the relaxation time modes for the different components overlap, assignment and separation is not unambiguously possible. Even though five different labels were used for the fitted components in Figure 5, an actual assignment of five components appears unreasonable. A classification into three different components appears more justified,

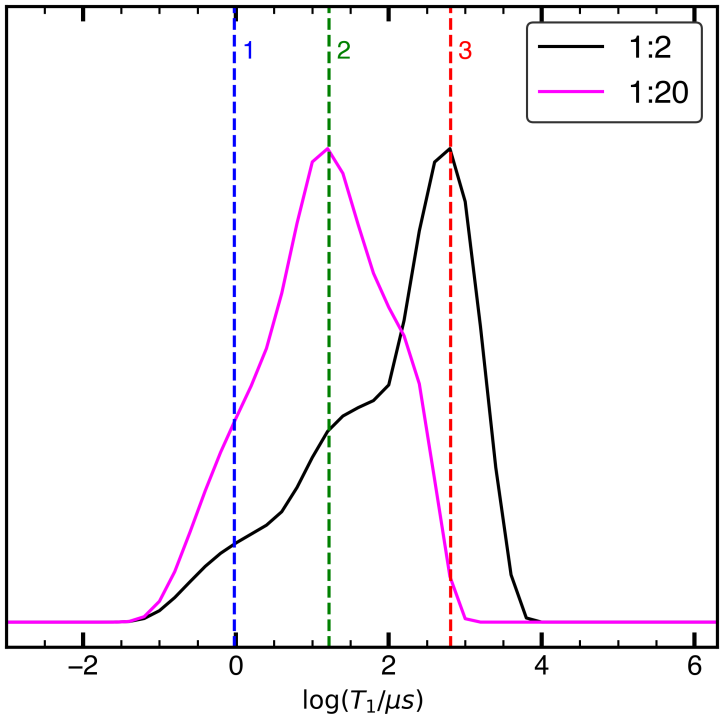

Figure 8: Comparison of relaxation time distributions for PTMA monomer to Super P ratios of 1:2 and 1:20. Inversion recovery experiments were conducted at 30 K and T_1 data was inverted using an exponential kernel to obtain the distributions. Dashed lines denote the three relaxation components resulting from different degree of PTMA monomer-Super P contact.

especially when considering the relaxation results at both temperatures. Furthermore, an exact Gaussian shape in log space for each of the modes is rather unlikely, yet such a fit provided a simple basis for the classification and discussion of the relaxation time distributions. It allowed rationalizing the origin of different relaxation components, and correlation of the composition with PTMA monomer–CB contact could be established by following apparent changes in the ILT-derived relaxation distributions. Therefore, the presented technique appears suitable as an analytical tool to compare different protocols for sample preparation.

Conclusion

The use of pulsed EPR relaxometry combined with Laplace inversion was demonstrated to characterize the contact between PTMA monomer and Super P carbon black in composite samples with varying PTMA monomer to Super P weight ratios. Inversion recovery

experiments revealed that sample composition and accessibility of the carbon black towards the PTMA monomer significantly affects the relaxation characteristics of the PTMA monomer. The time domain relaxation data was inverted using Inverse Laplace transform (ILT) to obtain relaxation time distributions, enabling the identification of different degrees of PTMA monomer–carbon black contact. ILT was found to be apt for detecting changes in the relaxation characteristics of nitroxides in the presence of carbon black and at different distributions of nitroxides within the composite sample. Thereby, pulsed EPR relaxometry showed a different contrast than CW EPR, making it a complementary technique to also identify sample changes that do not lead to an apparent variation in the CW EPR spectra. Different relaxation components differing by at least an order of magnitude were evident in the relaxation distributions and could be monitored for a range of PTMA monomer to carbon black weight ratios. Our analysis indicates that the composition of the sample significantly affects the quality of contact between the PTMA monomer and carbon black. Laplace inverted pulsed EPR relaxation may serve as a robust tool to study such contact also in other, similar systems.

Acknowledgements

The German research foundation (DFG) is acknowledged for funding within the priority program SPP 2248 Polymer-Based Batteries. The authors thank Dr. P. Philipp M. Schleker for valuable discussions.

References

[1] T. Placke, R. Kloepsch, S. Dühnen, M. Winter, *Journal of Solid State Electrochemistry* **2017**, *21*, 1939–1964.

[2] J. M. Tarascon, M. Armand, *Nature* **2001**, *414*, 359–367.

[3] E. Foreman, W. Zakri, M. Hossein Sanatimoghaddam, A. Modjtahedi, S. Pathak, A. G. Kashkooli, N. G. Garafolo, S. Farhad, *Advanced Sustainable Systems* **2017**, *1*, 1700061.

[4] G. Liu, H. Zheng, A. S. Simens, A. M. Minor, X. Song, V. S. Battaglia, *Journal of The Electrochemical Society* **2007**, *154*, A1129.

[5] M. D. Hager, B. Esser, X. Feng, W. Schuhmann, P. Theato, U. S. Schubert, *Advanced Materials* **2020**, *32*, 2000587.

[6] K. Nakahara, S. Iwasa, M. Satoh, Y. Morioka, J. Iriyama, M. Suguro, E. Hasegawa, *Chemical Physics Letters* **2002**, *359*, 351–354.

[7] H. Nishide, S. Iwasa, Y. J. Pu, T. Suga, K. Nakahara, M. Satoh, *Electrochimica Acta* **2004**, *50*, 827–831.

[8] D. R. Nevers, F. R. Brushett, D. R. Wheeler, *Journal of Power Sources* **2017**, *352*, 226–244.

[9] H. Hishide, T. Suga, *Electrochemical Society Interface* **2005**, *14*, 32–36.

[10] T. Janoschka, M. D. Hager, U. S. Schubert, *Advanced Materials* **2012**, *24*, 6397–6409.

[11] J. K. Kim, G. Cheruvally, J. H. Ahn, Y. G. Seo, D. S. Choi, S. H. Lee, C. E. Song, *Journal of Industrial and Engineering Chemistry* **2008**, *14*, 371–376.

[12] Q. Huang, D. Choi, L. Cosimbescu, J. P. Lemmon, *Physical Chemistry Chemical Physics* **2013**, *15*, 20921–20928.

[13] C. M. Liu, J. Chen, F. Q. Wang, B. L. Yi, *Russian Journal of Electrochemistry* **2012**, *48*, 1052–1057.

[14] S. Yoshihara, H. Isozumi, M. Kasai, H. Yonehara, Y. Ando, K. Oyaizu, H. Nishide, *Journal of Physical Chemistry B* **2010**, *114*, 8335–8340.

[15] M. Park, X. Zhang, M. Chung, G. B. Less, A. M. Sastry, *Journal of Power Sources* **2010**, *195*, 7904–7929.

[16] A. Vlad, J. Rolland, G. Hauffman, B. Ernould, J. F. Gohy, *ChemSusChem* **2015**, *8*, 1692–1696.

[17] G. Hauffman, Q. Maguin, J. P. Bourgeois, A. Vlad, J. F. Gohy, *Macromolecular Rapid Communications* **2014**, *35*, 228–233.

[18] C. H. Lin, J. T. Lee, D. R. Yang, H. W. Chen, S. T. Wu, *RSC Advances* **2015**, *5*, 33044–33048.

[19] S. Bahceci, B. Esat, *Journal of Power Sources* **2013**, *242*, 33–40.

[20] M. Khodeir, B. Ernould, J. Brassinne, S. Ghiassinejad, H. Jia, S. Antoun, C. Friebe, U. S. Schubert, Z. Kochovski, Y. Lu, E. V. Ruymbeke, J. F. Gohy, *Soft Matter* **2019**, *15*, DOI `10.1039/c9sm00905a`.

[21] C. Szczuka, J. Ackermann, P. P. M. Schleker, P. Jakes, R.-A. Eichel, J. Granwehr, *Communications Materials* **2021**, *2*, 20.

[22] I. Kulikov, N. A. Panjwani, A. A. Vereshchagin, D. Spallek, D. A. Lukianov, E. V. Alekseeva, O. V. Levin, J. Behrends, *Energy and Environmental Science* **2022**, *15*, 3275–3290.

[23] C. Szczuka, P. Jakes, R.-A. Eichel, J. Granwehr, *Advanced Energy and Sustainability Research* **2021**, *2*, 2100121.

[24] C. Szczuka, R.-A. Eichel, J. Granwehr, *ACS Applied Energy Materials* **2022**, *5*, 449–460.

[25] A. Niemöller, P. Jakes, S. Eurich, A. Paulus, H. Kungl, R. A. Eichel, J. Granwehr, *Journal of Chemical Physics* **2018**, *148*, 014705.

[26] A. Niemöller, P. Jakes, R. A. Eichel, J. Granwehr, *Scientific Reports* **2018**, *8*, 1–7.

[27] M. Sathiya, J. B. Leriche, E. Salager, D. Gourier, J. M. Tarascon, H. Vezin, *Nature Communications* **2015**, *6*, 6276.

[28] E. P. Kirilina, T. P. Prisner, M. Bennati, B. Endeward, S. A. Dzuba, M. R. Fuchs, K. Möbius, A. Schnegg, *Magnetic Resonance in Chemistry* **2005**, *43*, S119–S129.

[29] Y. N. Molin, K. M. Salikhov, K. I. Zamaraev in Springer Series in Chemical Physics, Springer Berlin Heidelberg, Berlin, Heidelberg, **1980**, pp. 11–106.

[30] Q. Huang, E. D. Walter, L. Cosimbescu, D. Choi, J. P. Lemmon, *Journal of Power Sources* **2016**, *306*, 812–816.

[31] K. Sheem, Y. H. Lee, H. S. Lim, *Journal of Power Sources* **2006**, *158*, 1425–1430.

[32] J.-L. Du, G. R. Eaton, S. S. Eaton, *Journal of Magnetic Resonance Series A* **1995**, *115*, 213–221.

[33] I. V. Koptyug, S. H. Bossmann, N. J. Turro, *Journal of the American Chemical Society* **1996**, *118*, 1435–1445.

[34] A. Schweiger, G. Jeschke, *Principles of Pulse Electron Paramagnetic Spectroscopy*, Oxford University Press, **2001**, p. 578.

[35] S. S. Eaton, G. R. Eaton in **2002**, pp. 29–154.

[36] R. L. Collins, M. D. Bell, G. Kraus, *Journal of Applied Physics* **1959**, *30*, 56–62.

[37] G. Wagoner, *Physical Review* **1960**, *118*, 647–653.

[38] C. Brosseau, P. Molinié, F. Boulic, F. Carmona, *Journal of Applied Physics* **2001**, *89*, 8297–8310.

[39] A. Watanabe, H. Ishikawa, K. Mori, O. Ito, *Carbon* **1989**, *27*, 863–867.

[40] J. F. Baugher, B. Ellis, *Journal of Colloid And Interface Science* **1972**, *38*, 658–659.

[41] L. S. Singer, G. Wagoner, *The Journal of Chemical Physics* **1962**, *37*, 1812–1817.

[42] G. Feher, A. F. Kip, *Physical Review* **1955**, *98*, 337–348.

[43] F. J. Dyson, *Physical Review* **1955**, *98*, 349–359.

[44] D. Pines, C. P. Slichter, *Physical Review* **1955**, *100*, 1014–1020.

[45] G. R. Eaton, S. S. Eaton in *Nitroxides*, Royal Society of Chemistry, Cambridge, **2021**, pp. 551–579.

[46] S. S. Eaton, G. R. Eaton in *eMagRes*, *Vol. 5*, 4, John Wiley & Sons, Ltd, Chichester, UK, **2016**, pp. 1543–1556.

[47] D. J. Lépine, *Physical Review B* **1970**, *2*, 2429–2439.

[48] D. V. Savchenko, E. N. Kalabukhova, A. Pöppl, E. N. Mokhov, B. D. Shanina, *Physica Status Solidi (B) Basic Research* **2011**, *248*, 2950–2956.

[49] D. V. Savchenko, *Journal of Applied Physics* **2015**, *117*, 045708.

[50] D. Savchenko, E. Kalabukhova, B. Shanina, S. Cichoň, J. Honolka, V. Kiselov, E. Mokhov, *Journal of Applied Physics* **2016**, *119*, 045701.

[51] A. Kulikov, G. Likhtenstein, *Advances in Molecular Relaxation and Interaction Processes* **1977**, *10*, 47–79.

[52] J. S. Hyde, K. V. Rao, *Journal of Magnetic Resonance (1969)* **1978**, *29*, 509–516.

[53] S. S. Eaton, G. R. Eaton, Determination of Distances Based on T1 and Tm Effects, **2002**.

[54] G. Jeschke, Y. Polyhach, *Physical Chemistry Chemical Physics* **2007**, *9*, 1895–1910.

[55] D. Bytchenkoff, S. Rodts, *Journal of Magnetic Resonance* **2010**, *208*, 4–19.

[56] J. Granwehr, W. Köckenberger, *Applied Magnetic Resonance* **2008**, *34*, 355–378.

[57] L. Venkataramanan, Y.-Q. Song, M. D. Hürlimann, *IEEE Trans. Signal Process.* **2002**, *50*, 1017–1026.

[58] Y. Q. Song, L. Venkataramanan, M. D. Hürlimann, M. Flaum, P. Frulla, C. Straley, *Journal of Magnetic Resonance* **2002**, *154*, 261–268.

[59] A. A. Istratov, O. F. Vyvenko, *Review of Scientific Instruments* **1999**, *70*, 1233–1257.

[60] G. C. Borgia, R. J. S. Brown, P. Fantazzini, *J. Magn. Reson.* **1998**, *132*, 65–77.

[61] J. Granwehr, P. J. Roberts, *Journal of Chemical Theory and Computation* **2012**, *8*, 3473–3482.

[62] M. Prange, Y.-Q. Song, *Journal of Magnetic Resonance* **2009**, *196*, 54–60.

[63] S. Merz, J. Wang, P. Galvosas, J. Granwehr, *Molecules* **2021**, *26*, 6690.

[64] I. Cho, J. Choi, K. Kim, M. H. Ryou, Y. M. Lee, *RSC Advances* **2015**, *5*, 95073–95078.

[65] H. B. Lin, W. Z. Huang, H. B. Rong, J. N. Hu, S. W. Mai, L. D. Xing, M. Q. Xu, X. P. Li, W. S. Li, *Journal of Power Sources* **2015**, *287*, 276–282.

[66] C Gemperle, G Aebli, A Schweiger, R. Ernst, *Journal of Magnetic Resonance (1969)* **1990**, *88*, 241–256.

[67] J. W. Eaton, D. Bateman, S. Hauberg, R. Wehbring, GNU Octave version 6.3.0 manual: a high-level interactive language for numerical computations, **2021**.

[68] B. Ellis, J. F. Baugher, *Journal of Polymer Science Part A-2: Polymer Physics* **1973**, *11*, 1461–1463.

[69] E. Bordignon in *eMagRes*, John Wiley & Sons, Ltd, Chichester, UK, **2017**, pp. 235–254.

[70] J. R. Klauder, P. W. Anderson, *Physical Review* **1962**, *125*, 912–932.

[71] Y. V. Toropov, S. A. Dzuba, Y. D. Tsvetkov, V. Monaco, F. Formaggio, M. Crisma, C. Toniolo, J. Raap, *Applied Magnetic Resonance* **1998**, *15*, 237–246.

[72] S. Agnello, R. Boscaino, M. Cannas, F. M. Gelardi, *Physical Review B* **2001**, *64*, 174423.

[73] S. Stoll, *eMagRes*, Major Reference Works **2017**, 23–38.

[74] Q. Zhang, Z. Yu, P. Du, C. Su, *Recent Patents on Nanotechnology* **2010**, *4*, 100–110.

Laplace inverted pulsed EPR relaxation to study contact between active material and carbon black in Li-organic battery cathodes

Davis Thomas Daniel[1,2,*],Conrad Szczuka[1], Peter Jakes[1], Rüdiger-A. Eichel[1,3], Josef Granwehr [1,2]

[1]Institute of Energy and Climate Research (IEK-9), Forschungszentrum Jülich, Jülich 52425, Germany
[2] Institute of Technical and Macromolecular Chemistry, RWTH Aachen University,Aachen 52056, Germany
[3] Institute of Physical Chemistry, RWTH Aachen University,Aachen 52056, Germany
**Correspondence to: d.daniel@fz-juelich.de*

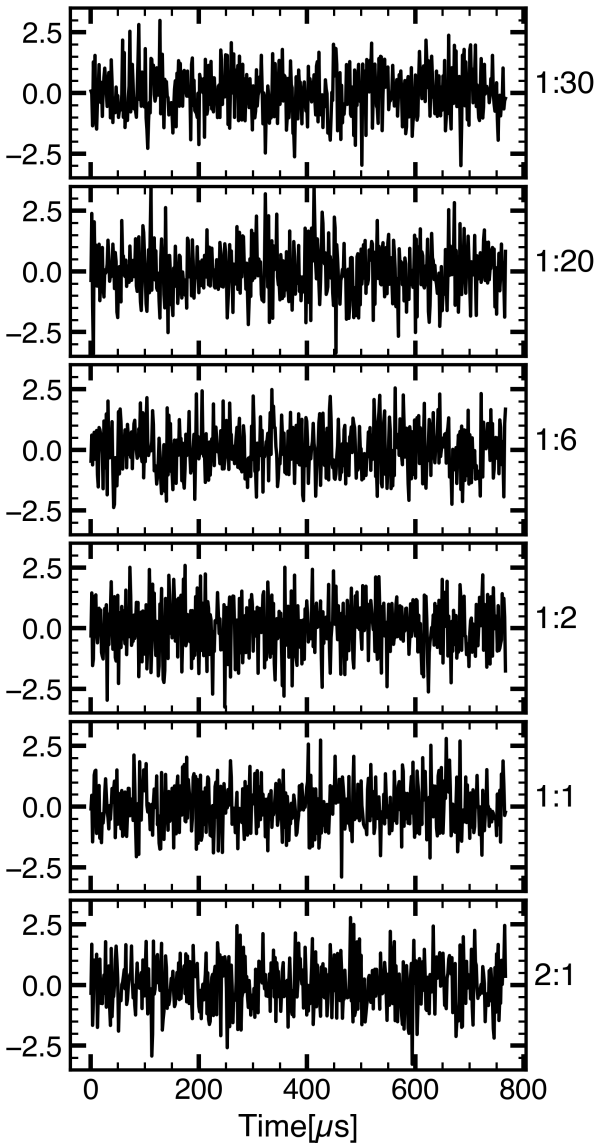

Figure S1: Residuals from ILT fits of T_1 data using an exponential kernel. The corresponding distributions are shown in Figure 5 of the main text. Ratios on the right edge denote the PTMA monomer to Super P weight ratio. The residuals were representative of random noise and did not show any apparent systematic features.

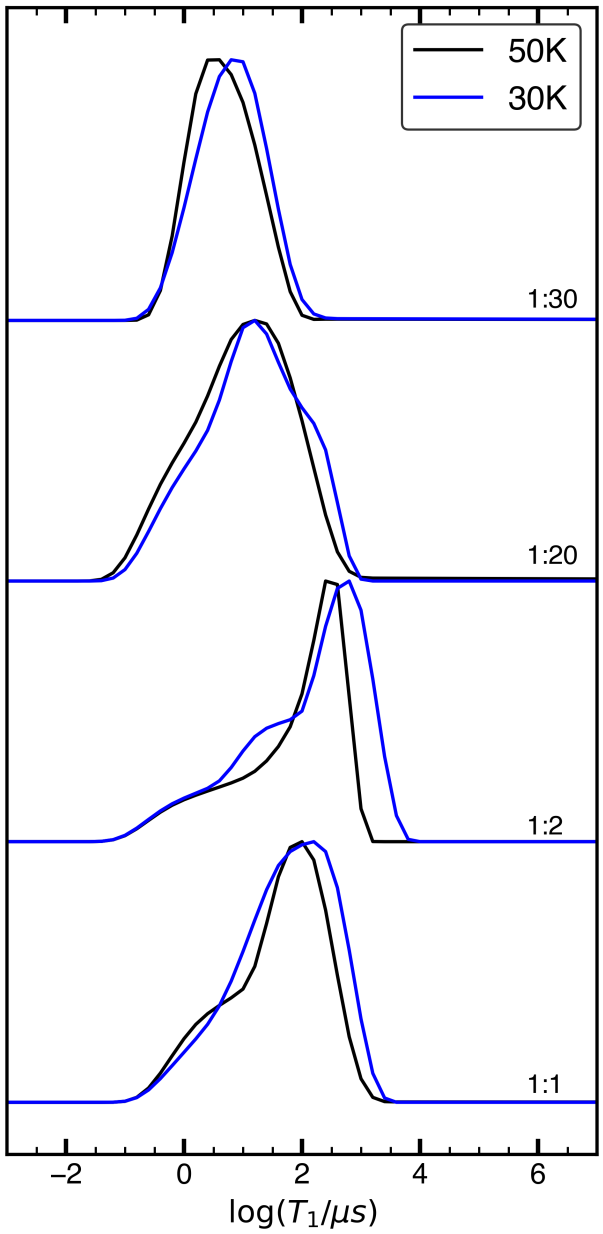

Figure S2: Comparison of Relaxation time distributions at 30 K (blue) and 50 K (black), obtained using ILT for composite samples. Ratios on the right edge denote the PTMA monomer to Super P weight ratio. The T_1 distribution at 30 K shows more resolved components and shift of the slower relaxing component.